Research Article

Novel oxidative *in vitro* metabolites of the mycotoxins alternariol and alternariol methyl ether

Erika Pfeiffer[1], Nils H. Schebb[1]*, Joachim Podlech[2] and Manfred Metzler[1]

[1] Institute of Applied Biosciences, University of Karlsruhe, Karlsruhe, Germany
[2] Institute of Organic Chemistry, University of Karlsruhe, Karlsruhe, Germany

The *Alternaria* toxins alternariol (AOH; 3,7,9-trihydroxy-1-methyl-6*H*-benzo[*c*]chromen-6-one) and alternariol methyl ether (AME, 3,7-dihydroxy-9-methoxy-1-methyl-6*H*-benzo[*c*]chromen-6-one) are common contaminants of food and feed, but their oxidative metabolism in mammals is as yet unknown. We have therefore incubated AME and AOH with microsomes from rat, human, and porcine liver and analyzed the microsomal metabolites with HPLC and GC-MS/MS. Seven oxidative metabolites of AME and five of AOH were detected. Their chemical structures were derived from their mass spectra using deuterated trimethylsilyl (TMS) derivatives, and from the information obtained from enzymatic methylation. Several of the metabolites were identified by comparison with synthetic reference compounds. AME as well as AOH were monohydroxylated at each of the four possible aromatic carbon atoms and also at the methyl group. In addition, AME was demethylated to AOH and dihydroxylated to a small extent. As the four metabolites arising through aromatic hydroxylation of AME and AOH are either catechols or hydroquinones, the oxidative metabolism of these mycotoxins may be of toxicological significance.

Keywords: Alternariol / Alternariol methyl ether / Microsomes / Oxidative metabolites

Received: November 15, 2006; revised: Decmeber 15, 2006; accepted: December 15, 2006

1 Introduction

Fungi of the genus *Alternaria* not only infest numerous food items but also grow on other materials, *e.g.*, soil, wallpapers, and textiles. *Alternaria alternata* is the most abundant of more than 40 *Alternaria* species and produces several toxins including alternariol (AOH, Fig. 1) and alternariol methyl ether (AME, Fig. 1). These *Alternaria* toxins are frequently detected in moldy wheat and other grains, in pecans, in various fruits, *e.g.* tomatoes, olives, melons, apples, and raspberries, and in processed fruit products such as apple and tomato juice [1]. Consumption of food contaminated with *Alternaria* toxins has been associated with an increased incidence of esophageal cancer [2], and there are several reports on the mutagenicity and genotoxicity of AOH and AME [3 – 6].

Although AOH and AME are common contaminants of food and feed, very little is known about the fate of these mycotoxins in the mammalian organism. No studies have yet been published on the metabolism of AOH, whereas two reports exist on the disposition of AME. Pollock *et al.* [7] incubated AME with rat liver postmitochondrial supernatant and showed, by TLC, the formation of AOH and several polar metabolites of unknown structure. Similar polar products were detected in feces and urine of intact rats after oral administration of AME [7]. When AME was incubated with the homogenate from female porcine liver and mucosa, AOH was detected as a metabolite arising through demethylation of AME, and a high activity for glucuronidation of AME was observed for both homogenates [8].

It was the objective of the present study to elucidate the chemical structures of the microsomal metabolites of AME and AOH. Five monohydroxylated metabolites were formed from each mycotoxin in rat, porcine, and human hepatic microsomes, and their structures were assigned by GC-MS/MS analysis, enzymatic derivatization, and, in part, comparison with reference compounds.

Correspondence: Dr. Manfred Metzler, Institute of Applied Biosciences, Sections of Food Chemistry and Food Toxicology, University of Karlsruhe, P.O. Box 6980, D-76128 Karlsruhe, Germany
E-mail: Manfred.Metzler@chemie.uni-karlsruhe.de
Fax: +49-721-608-7255

Abbreviations: AOH, alternariol; **AME,** alternariol methyl ether; **COMT,** catechol-*O*-methyltransferase; **EI**, electron impact; **MP,** methylation product; **NADPH,** nicotinamide adenine dinucleotide phosphate, (reduced form); **SAM,** *S*-adenosyl-L-methionine; **TMS,** trimethylsilyl

* This work represents the Diploma thesis of Nils H. Schebb.

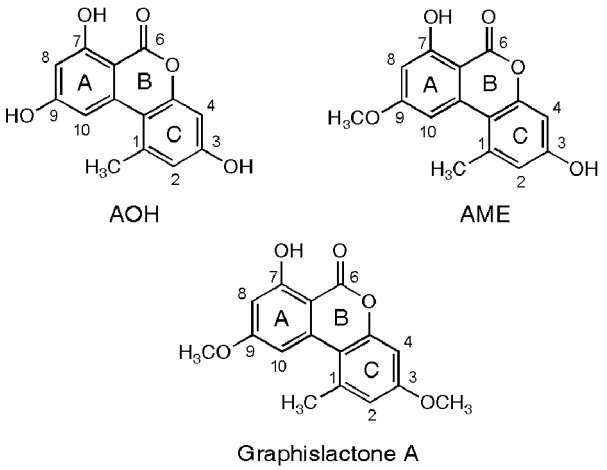

Figure 1. Chemical structures of AOH, AME, and graphislactone A.

2 Materials and methods

2.1 Chemicals, animals, and cell fractions

AME was purchased from Sigma/Aldrich/Fluka (Taufkirchen, Germany) and had a purity of >96% according to HPLC analysis, containing 2.2% AOH. AOH was synthesized in the laboratory of J. Podlech as previously reported [9], and contained 1.1% AME as determined by HPLC. Graphislactone A, which is 4-hydroxy-3,9-*O*-dimethyl-AOH, was also synthesized in the laboratory of J. Podlech and characterized by NMR spectroscopy. ^{1}H NMR (400 MHz, DMSO-d_6): δ 2.70 (s, 3H, CH_3), 3.88 (s, 3H, OCH_3), 3.90 (s, 3H, OCH_3), 6.60 (d, 1H, ^{4}J = 2.2 Hz, aryl-*H*), 6.92 (s, 1H, aryl-*H*), 7.20 (d, 1H, ^{4}J = 2.2 Hz, aryl-*H*), 9.24 (s, 1H, O*H*), 11.87 (s, 1H, O*H*). ^{13}C NMR (101 MHz, DMSO-d_6): δ 24.6 (q), 55.7 (q), 55.9 (q), 98.4 (s), 99.4 (d), 103.8 (d), 110.5 (s), 112.9 (d), 126.1 (s), 132.3 (s), 137.9 (s), 140.6 (s), 148.1 (s), 164.0 (s), 164.4 (s), 166.0 (s). The demethylation of graphislactone A with boron tribromide yielded a mixture of 4-hydroxy-AME and 4-hydroxy-AOH which were distinguished by HPLC and GC-MS/MS after trimethylsilylation. Nicotinamide adenine dinucleotide phosphate (NADP$^+$), *S*-adenosyl-L-methionine (SAM), *N*,*O*-bis(trimethylsilyl)trifluoroacetamide (BSTFA), and other chemicals and reagents were of the highest quality available and were purchased from Sigma/Aldrich/Fluka. *N*,*O*-Bis(d9-trimethylsilyl)acetamide (d9-BSA) was from Campro Scientific (Berlin, Germany) and HPLC-grade ACN from Carl Roth (Karlsruhe, Germany).

Male Sprague–Dawley rats were purchased from Harlan Winkelmann (Borchen, Germany). Animals were kept under a 12 h light/dark cycle and received water and commercial lab chow *ad libitum*. Microsomes were prepared from the livers of untreated male rats with 200–300 g weight and of adult female pigs immediately after slaughter, as well as from the liver of a 63-year-old male white human (kindly provided by Dr. J. Weymann, formerly with Knoll AG, Ludwigshafen, Germany), as described by Lake [10]. Protein concentrations were measured according to Bradford [11] with BSA as standard. The concentration of active cytochrome P450, determined by the method of Omura and Sato [12], was 0.84, 0.39, and 0.20 nmol/mg protein in rat, porcine, and human liver microsomes, respectively. Rat liver cytosol, obtained as the 100 000 × *g* supernatant of the microsomal preparation, was used as source of catechol-*O*-methyltransferase (COMT).

2.2 Microsomal incubations

Oxidative *in vitro* metabolism of AME and AOH was studied by incubating microsomes (0.7–1 mg microsomal protein/mL) with 50 μM substrate dissolved in DMSO (final concentration 0.5–1%) and a nicotinamide adenine dinucleotide phosphate (reduced form) (NADPH)-generating system (0.9 U isocitrate dehydrogenase, 9.4 mM isocitrate, 1.21 mM NADP$^+$, and 4.3 mM magnesium chloride) in a final volume of 1 mL of 0.1 M phosphate buffer at pH 7.4. After preincubation for 5 min at 37°C, the NADPH-generating system was added and the mixture incubated for 40 min at 37°C. Subsequently, the incubation mixture was extracted with 3 × 0.5 mL ethyl acetate and the pooled extract evaporated to dryness. The residue was dissolved in 50 μL methanol for HPLC and GC-MS analyses. Control incubations were carried out with heat-inactivated microsomes, or with intact microsomes but without a NADPH-generating system.

2.3 Incubations with COMT

Oxidative metabolites of AME and AOH, extracted from the microsomal incubations and fractionated by HPLC (see below), were dissolved in DMSO and added to 250 μL of 0.1 M phosphate buffer at pH 7.4 containing 0.1 M magnesium chloride and 10 μL of rat liver cytosol. The concentration of DMSO in the final incubation did not exceed 1%. After 5 min incubation at 37°C, 7 μL of a 20 mM solution of SAM in phosphate buffer was added and the incubation continued for another 30 min. Control incubations were run without SAM. The aqueous incubation mixtures were then extracted with ethyl acetate and processed as described for the microsomal incubations.

2.4 HPLC analysis

A Beckman system equipped with a binary pump, a photodiode array detector, and 32 Karat 7.0 software for data collection and analysis was used. Separation was carried out on a 250 mm × 4.6 mm id, 5 μm, RP Luna C8 column (Phenomenex, Torrance, CA, USA). Solvent A was deionized water adjusted to pH 3.0 with formic acid, and solvent B

was ACN. A linear solvent gradient was started 2 min after injection, changing from 17% B to 45% B in 7 min, then to 50% B in 7 min, then to 100% B in 14 min. After 4 min of eluting the column with 100% B, the initial 17% B was reached in 5 min. The flow rate was 1 mL/min and the detector was set to 254 nm. HPLC fractions of the metabolites were collected, extracted with ethyl acetate, and used for GC-MS/MS analysis or for incubations with COMT.

2.5 GC-MS/MS analysis

A Finnigan GCQ capillary gas chromatograph equipped with a 30 m × 0.25 mm id, 0.25 µm, 5% phenylmethyl MDN-5S fused-silica column (Supelco, Bellefonte, PA, USA) and coupled to an IT detector, was operated with electron impact (EI) ionization at 70 eV (Thermo Finnigan, Austin, TX, USA). Samples dissolved in methanol or ethyl acetate were evaporated to dryness, dissolved in 30 µL of BSTFA or d9-BSA, and 1 µL was injected, using the splitless mode for 90 s. The injection port temperature was 50°C at the time of injection and, after 30 s, raised to 275°C at 8°C/min. The oven temperature was programmed from 60°C (1 min hold) to 290°C (15 min hold) at a rate of 15°C/min. The transfer line and ion source were kept at 275 and 250°C, respectively. Helium was used as carrier gas with a flow rate of 40 cm/s. Mass spectra were scanned from *m*/*z* 50 to 650 at a rate of 0.5 s/scan. For MS/MS analysis, an additional voltage of 1.5 V was applied to the end caps of the IT to induce fragmentations.

3 Results

3.1 Oxidative metabolites of AME

Microsomes from the livers of male Sprague – Dawley rats were incubated with AME in the presence of an NADPH-generating system and subsequently extracted with ethyl acetate. Analysis of the extract by RP-HPLC with DAD revealed the presence of five peaks which eluted earlier than AME and were not observed in control experiments with heat-inactivated microsomes or in the absence of the NADPH-generating system (Fig. 2). The HPLC retention times of these five metabolites, which were eventually identified as four monohydroxylated and one dihydroxylated AME as described below, are listed in Table 1. In addition, AOH was found both in complete and in control incubations, due to the presence of AOH as an impurity in AME. The UV spectra of the five new metabolites were very similar to that of AME, with maxima of absorbance at 257, 288, 300, and 340 nm (data not shown). In order to elucidate the chemical structures of the AME metabolites, the extract was trimethylsilylated with normal as well as perdeuterated silylating agent and analyzed by GC-MS.

Table 1. Chromatographic properties of the oxidative metabolites of AME and AOH as well as their MPs obtained by incubation with COMT

Metabolite	Retention time (min)		MP (position of methyl group: GC retention-time in min; approximate ratio of MPs)
	HPLC	GC[a)]	
AME	20.9	21.1	na[b)]
AOH	15.3	21.1	na
Dihydroxy-AME	11.1	nd[c)]	nc[d)]
8-Hydroxy-AME	13.8	22.6	C-8: 22.2; C-7[e)]: 22.9; C-8/C-7 ≈ 10 : 1
10-Hydroxy-AME	16.2	19.1	No reaction with COMT
4-Hydroxy-AME	16.9	20.9	C-4: 20.8; C-3[f)]: 21.3; C-4/C-3 ≈ 1 : 8
2-Hydroxy-AME[g)]	18.8	23.3	MP-1: 20.9; MP-2: 23.6; MP-1/MP-2 ≈ 1 : 1
Methyl-hydroxy-AME	nd	22.1	nc
AOH	15.3	21.1	na
8-Hydroxy-AOH	12.3	22.1	C-9[h)]: 22.6; only 1 MP found in GC-MS/MS
4-Hydroxy-AOH[i)]	12.8	20.9	MP-1: 21.4; MP-2: 21.8; MP-1/MP-2 ≈ 1 : 9
10-Hydroxy-AOH	13.4	19.3	C-9[j)]: 19.1; only 1 MP found in GC-MS/MS
2-Hydroxy-AOH	13.8	23.4	MPs not resolved in GC: broad peak at 22.1
Methyl-hydroxy-AOH	14.8	22.3	nc

a) TMS derivatives.
b) na, not applicable.
c) nd, not detected.
d) nc, not conducted.
e) This MP did not give a $[M-15]^+$ ion in GC-MS.
f) This MP had identical GC retention time and GC-MS/MS data with graphislactone A.
g) Sites of methylation could not be assigned.
h) This MP had identical GC retention time and GC-MS/MS data with 8-hydroxy-AME.
i) Sites of methylation could not be assigned.
j) This MP had identical GC retention time and GC-MS/MS data with 10-hydroxy-AME.

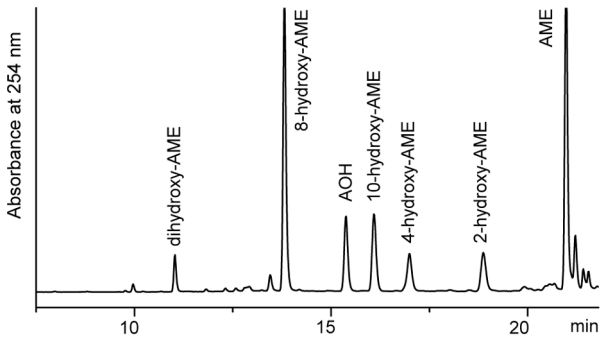

Figure 2. HPLC profile of the extract from the incubation of AME with NADPH-fortified rat liver microsomes.

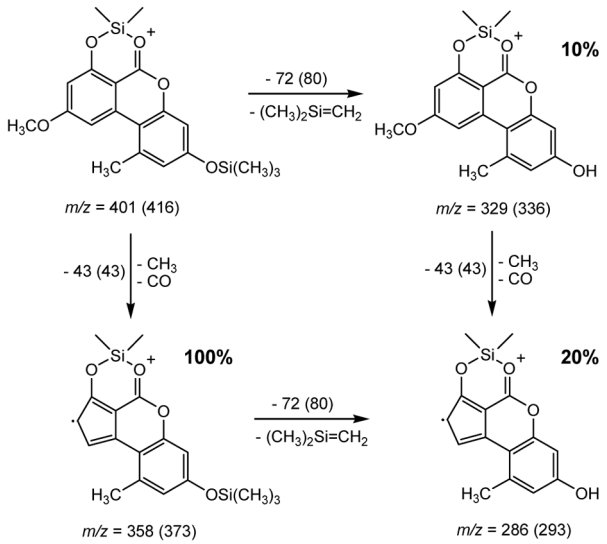

Figure 3. Proposed fragmentation of the $[M-15]^+$ ion (*m*/*z* 401) of trimethylsilylated AME. Percent values denote relative abundance. Values in parentheses denote *m*/*z* of the perdeutero-TMS derivative.

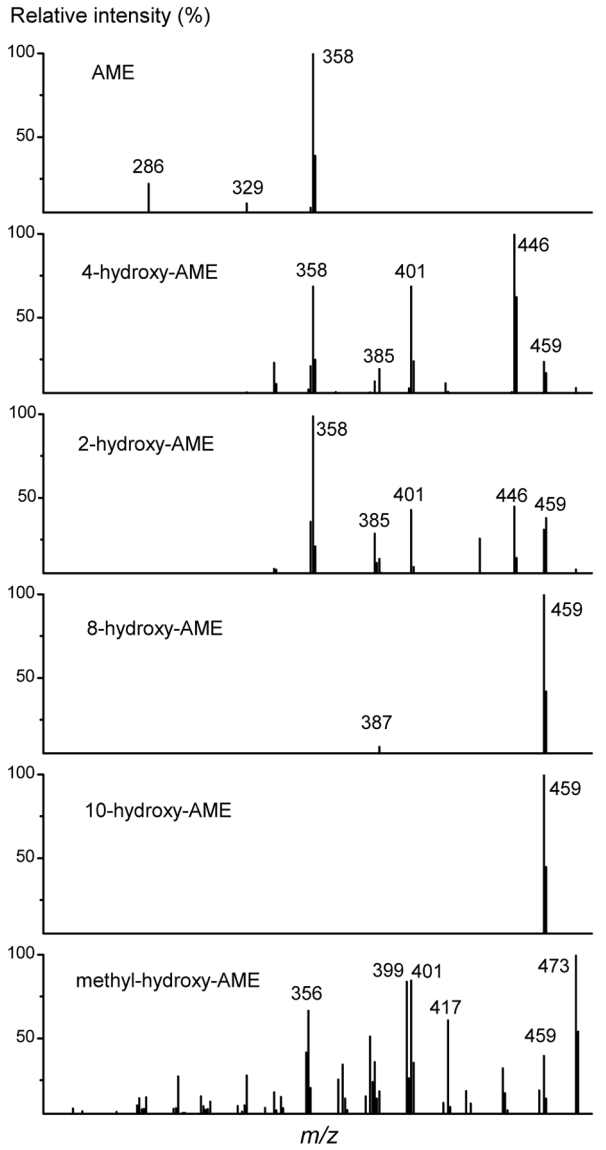

Figure 4. Daughter ion spectra of the TMS derivatives of AME (parent ion *m*/*z* 401) and its monohydroxylated metabolites (parent ion *m*/*z* 489).

Pilot studies with AME had shown that both hydroxyl groups are trimethylsilylated and the EI mass spectrum obtained by GC-MS exhibits no molecular ion but a very intense ion at *m*/*z* 401, representing the $[M-15]^+$ ion (data not shown). Because the corresponding ion in the mass spectrum of the perdeutero-trimethylsilylated AME appears at *m*/*z* 416 indicating the loss of one perdeuterated methyl group, we propose the structure depicted in Fig. 3 for the ion *m*/*z* 401. No other fragment ions with decent intensities were observed in the mass spectrum. However, when the ion *m*/*z* 401 was subjected to collision-induced fragmentation, ions at *m*/*z* 358, 329, and 286 appeared in the daughter ion spectrum (Fig. 4). The proposed formation of these ions is shown in Fig. 3: the loss of 43 amu leading to *m*/*z* 358 involves cleavage of methyl from the methoxyl group, followed by elimination of carbon monoxide and formation of a five-membered ring, which is part of a very stable polycyclic system. A subsequent minor fragmentation is the elimination of $(CH_3)_2Si=CH_2$ from the trimethylsilyl (TMS) group leading to *m*/*z* 286. This ion can also arise through elimination of $(CH_3)_2Si=CH_2$ from *m*/*z* 401 to yield *m*/*z* 329, followed by loss of 43 amu. The proposed fragmentations are consistent with the ions found in the daughter ion spectra in the perdeutero-trimethylsilylated AME (Fig. 3).

When the extract containing the microsomal AME metabolites was analyzed by GC-MS after trimethylsilylation, five peaks of the TIC contained a prominent ion at *m*/*z* 489, which corresponds to the $[M-15]^+$ of the TMS derivative of monohydroxylated AME. Their GC retention times are listed in Table 1, together with the tentative chemical structures. Four of the five GC peaks containing monohydroxy-

lated AME were correlated with their corresponding HPLC peak by collecting each HPLC peak and subjecting it to GC-MS. In addition to the four monohydroxylated AME metabolites detected in HPLC, a small amount of a fifth monohydroxylation product was observed in GC-MS which could not be seen in HPLC.

The structure elucidation of the five monohydroxylated AME metabolites is based on the daughter ion spectra of their TMS derivatives obtained in GC-MS/MS, utilizing the mass differences between corresponding ions from trimethylsilylated and perdeutero-trimethylsilylated metabolites. In addition, subsequent reactions with the enzyme COMT were conducted, taking advantage of the fact that three of the conceivable monohydroxylation products of AME are catechols.

Upon MS/MS of the *m/z* 489 ions in those five metabolite peaks, the daughter ion spectra depicted in Fig. 4 were obtained. It was obvious that there were two pairs of similar spectra, whereas the fifth spectrum was quite different. The spectrum of the TMS derivative of 4-hydroxy-AME contained the ions *m/z* 401 and 358, which were also found in the MS and MS/MS, respectively, of the parent AME (see above). However, the corresponding ions of the deuterated TMS derivatives of the metabolites, *i.e.* *m/z* 413 and 370, were not identical with those of the deuterated AME, *i.e.* *m/z* 416 and 373 (Fig. 3). The proposed fragmentation of 4-hydroxy-AME, which also accounts for the formation of *m/z* 446, is depicted in Fig. 5. In addition to the loss of 43 amu, already discussed above for AME, the loss of 88 amu is dominant in the fragmentation of trimethylsilylated 4-hydroxy-AME. The latter is due to the elimination of tetramethylsilane, which is characteristic of two vicinal trimethylsilylated phenolic hydroxyl groups [13, 14]. This and the loss of 43 amu, indicating an unchanged ring A, suggested a catechol structure at ring C. Definitive evidence for the structure of 4-hydroxy-AME was provided by comparison with an authentic reference compound, obtained by chemical demethylation of graphislactone A, which is 3-*O*-methyl-4-hydroxy-AME. The microsomal 4-hydroxy-AME and the standard 3-*O*-desmethyl graphislactone A had identical mass spectra and retention times in GC and HPLC. Moreover, both compounds gave rise to the same products after methylation with COMT (Table 1).

The daughter ion spectrum of the TMS derivative of 2-hydroxy-AME is very similar to that of 4-hydroxy-AME, sharing the ions *m/z* 446, 401, and 358 (Fig. 4). The unchanged ring A, loss of 88 amu, and reaction with COMT (Table 1) strongly suggests a catechol structure at ring C. Thus, the newly introduced hydroxyl group must be located at C-2.

The daughter ion spectra of the trimethylsilylated HPLC peaks eluting at both 13.8 and 16.2 min exhibited a very intense ion at *m/z* 459 with a very small ion at *m/z* 387 and virtually no further fragments (Fig. 4). Taking into account the lack of elimination of 43 and 88 amu and the corresponding ions of the deuterated TMS derivatives, hydroxylation at ring A next to the methoxyl group had to be assumed. The dominant loss of 30 amu from the $[M-15]^+$ ion *m/z* 489 to yield *m/z* 459 and the concomitant loss of three deuterium atoms can be explained by the elimination of ethane, containing one methyl from the TMS group and the other methyl from the methoxyl group (Fig. 6). The two possible hydroxylation products of AME at ring A could be discriminated by their reaction with COMT: only the metabolite eluting at 13.8 min in HPLC gave rise to two methylation products (MPs), indicating a catechol structure and therefore representing 8-hydroxy-AME, whereas the metabolite at 16.2 min was not methylated by COMT and must therefore be 10-hydroxy-AME (Table 1).

The very small GC peak of the fifth monohydroxylation product of AME provided a much more complex daughter ion spectrum of the ion at *m/z* 489, displaying ions resulting from the loss of 90 amu, *i.e.*, trimethylsilanol, yielding *m/z* 399 and subsequently 43 amu to yield *m/z* 356. Also,

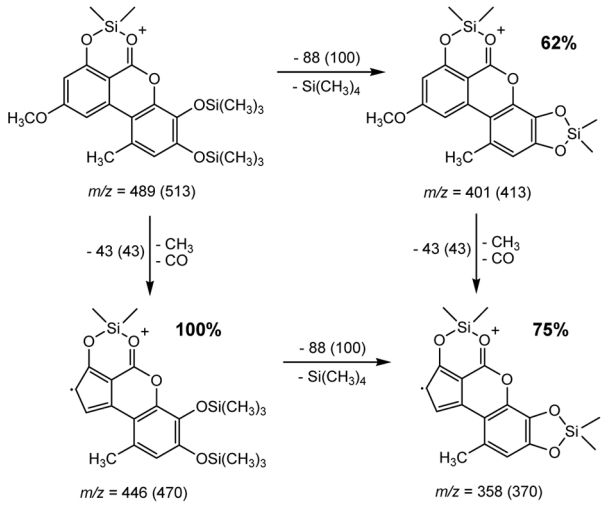

Figure 5. Proposed fragmentation of the $[M-15]^+$ ion (*m/z* 489) of the trimethylsilylated AME metabolite eventually identified as 4-hydroxy-AME. Percent values denote relative abundance. Values in parentheses denote *m/z* of the perdeutero-trimethylsilyl derivative.

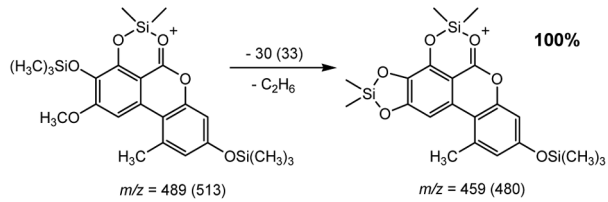

Figure 6. Proposed fragmentation of the $[M-15]^+$ ion (*m/z* 489) of the trimethylsilylated AME metabolite eventually identified as 8-AME. Percent values denote relative abundance. Values in parentheses denote *m/z* of the perdeutero-TMS derivative.

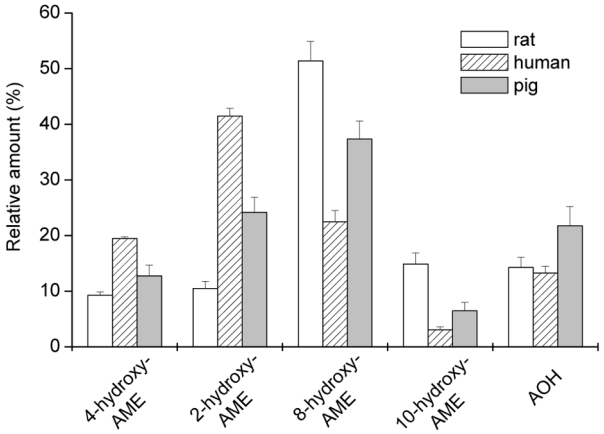

Figure 7. Pattern of oxidative AME metabolites generated with liver microsomes from rat, human, and pig. The concentration of AME was 50 μM and did not saturate the hydroxylation reaction. Total formation of hydroxylated metabolites was 295 ± 47.7, 679 ± 89.3, and 559 ± 98.8 pmol/min/nmol cytochrome P450 with microsomes from rat, human, and pig, respectively. Data represent mean ± SD from three independent experiments. Data for AOH are corrected for the amount present as impurity in AME.

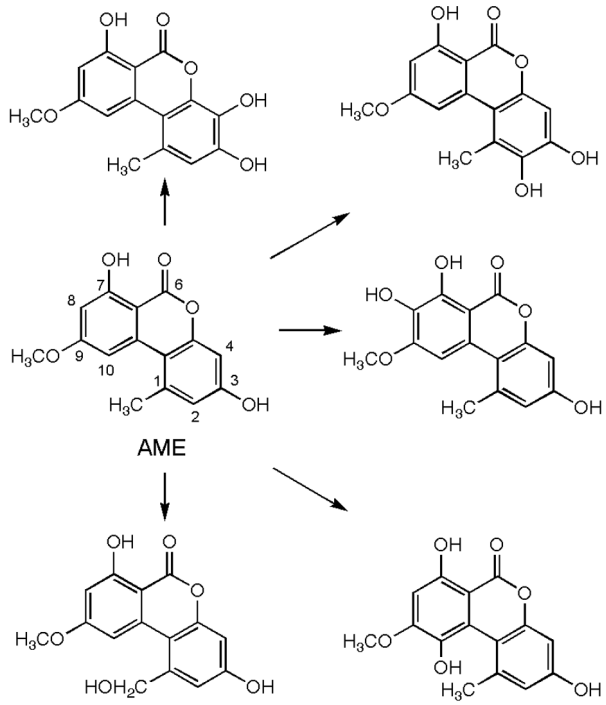

Figure 8. Oxidative metabolism of AME.

loss of 72 amu, *i.e.*, $(CH_3)_2Si{=}CH_2$, from *m/z* 489 to give *m/z* 417 was observed. A possible structure is that of AME hydroxylated at the methyl group of C-1, which is also the only position left for monohydroxylation to a stable metabolite.

Although the AME used for microsomal hydroxylation contained 2.2% AOH, a quantitative account of the products showed that the amount of AOH had increased to about 7% during microsomal incubation. Thus, it must be assumed that demethylation of the methoxyl group takes place as a further oxidative pathway. The metabolic formation of AOH from AME is the only oxidative pathway reported in the literature to date [7, 8].

When the extract of the microsomal incubation was subjected to LC-MS analysis using positive ionization electrospray, the most polar metabolite gave rise to a prominent ion at m/z 305, which would be the $[M + H]^+$ ion of a dihydroxylated AME, whereas the mass spectra of the other four metabolites had intense ions at *m/z* 289 and low intensity ions at *m/z* 311, corresponding to the $[M + H]^+$ and $[M + Na]^+$ ions, respectively, of monohydroxylated AME. Thus, LC-MS analysis confirmed the presence of four monohydroxylated metabolites of AME. The exact structure of the minor dihydroxylated AME metabolite remains unknown.

In addition to the mono- and dihydroxylated metabolites of AME, several small peaks eluting after AME were observed in the HPLC profile of the extract from the microsomal incubation (not depicted in Fig. 2). The UV spectra of these unpolar products were very similar to that of AME. It is assumed that they represent dimers or trimers arising from oxidation products of the parent as well as hydroxylated AME, *e.g.*, phenoxy radicals, semiquinones, and quinones. Because these oligomers are probably artifacts of the *in vitro* incubation and do not form *in vivo*, no efforts were made to elucidate their structures.

AME was also incubated with microsomes from human and porcine liver in the presence of a NADPH-regenerating system and the extracted metabolites were analyzed by HPLC. No dihydroxylated AME was observed, but all the four aromatic monohydroxylation products generated with rat hepatic microsomes were also found in the incubations of AME with human and porcine liver microsomes (Fig. 7). However, there were marked differences in the amounts of the metabolites, in particular between human and rat liver microsomes.

In summary, our study has shown that AME is metabolized by rat, human, and porcine liver microsomes mostly to the four aromatic hydroxylation products 2-hydroxy-AME, 4-hydroxy-AME, 8-hydroxy-AME, and 10-hydroxy-AME, three of which are catechols (Fig. 8).

3.2 Oxidative metabolites of AOH

AOH was incubated with rat hepatic microsomes and the extracted metabolites were analyzed by HPLC and GC-MS/MS in the same manner as conducted with AME. The HPLC profile of the extract is depicted in Fig. 9. Five compounds not found in control incubations eluted faster than AOH from the RP column and had UV spectra virtually

identical with that of AOH (spectra not shown). The EI mass spectrum of trimethylsilylated AOH (spectrum not shown) did not exhibit a molecular ion at *m/z* 474 but had its base ion at *m/z* 459, arising through the loss of one methyl from a TMS group as indicated by the loss of three deuterium atoms in the spectrum of the perdeutero-trimethylsilylated AOH. As in the case of AME (see Fig. 3), formation of a siloxane ring involving C-6 and C-7 is therefore assumed. The EI mass spectra of the TMS derivatives of all the five metabolites exhibited their base ion at *m/z* 547, which represents the $[M-15]^+$ ion of monohydroxylated AOH, and did not exhibit a molecular ion (spectra not shown). When *m/z* 547 was subjected to collision-induced fragmentation, four of the AOH metabolites gave rise to the ions *m/z* 459 and 387, whereas the fifth metabolite had ions at *m/z* 457 and 385 (Fig. 10). The ions at *m/z* 459 indicate the loss of 88 amu, *i.e.*, tetramethylsilane, from the $[M-15]^+$ ion, which is typical for vicinal trimethylsilylated hydroxyl groups, as discussed above for the corresponding AME metabolites. As four of the AOH metabolites undergo this fragmentation, it is proposed that four catechols are generated in the microsomal metabolism of AOH by hydroxylation at the positions 2, 4, 8, and 10. The ion at *m/z* 387 arises from *m/z* 459 through the elimination of 72 amu, *i.e.*, $(CH_3)_2Si{=}CH_2$. These fragmentations are depicted for the TMS derivative of 4-hydroxy-AOH in Fig. 11, but also occur in the other AOH metabolites with a catechol structure. In two of the catechols, the release of 72 amu from *m/z* 547, leading to *m/z* 475, can precede the elimination of tetramethylsilane (Fig. 11).

It is not possible to derive the final structures of the four catechol metabolites, *i.e.*, the position of hydroxylation, from the daughter ion spectra because of their similarity. However, one of the metabolites could be identified as 4-hydroxy-AOH by comparison with a reference substance obtained by a complete chemical demethylation of graphislactone A. The AOH metabolite and the *bis*-demethylated graphislactone A had identical HPLC and GC retention times and daughter ion spectra. The structure of the other monohydroxylation product of ring C, *i.e.*, 2-hydroxy-

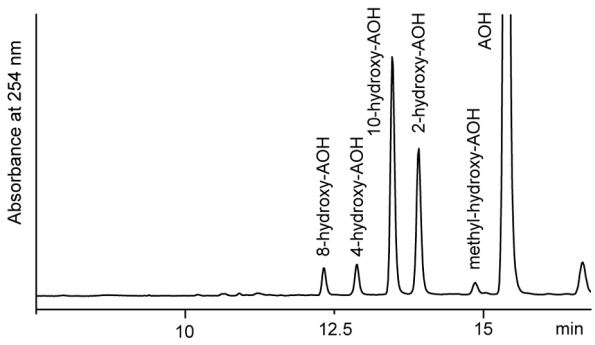

Figure 9. HPLC profile of the extract from the incubation of AOH with NADPH-fortified rat liver microsomes.

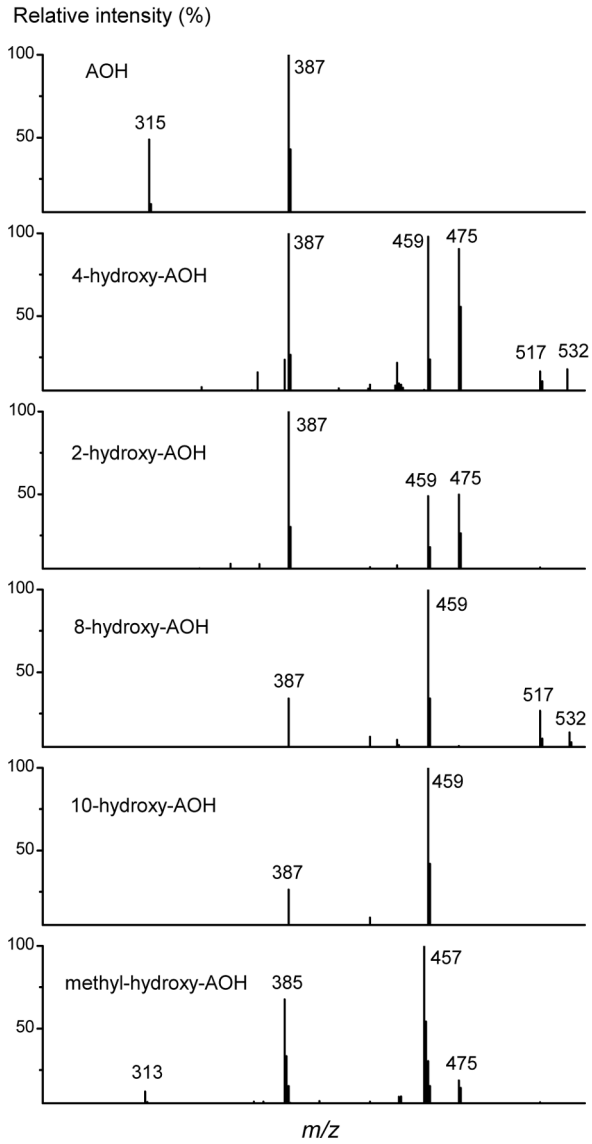

Figure 10. Daughter ion spectra of the TMS derivatives of AOH (parent ion *m/z* 459) and its monohydroxylated metabolites (parent ion *m/z* 547).

AOH, was assigned to the metabolite with the most similar daughter ion spectrum (Fig. 10). The remaining two catechol metabolites of AOH must then carry the newly introduced hydroxyl group at ring A. Discrimination of 8-hydroxy-AOH and 10-hydroxy-AOH was possible after their methylation with COMT. Although both ring A catechols were poor substrates of COMT, one of them was methylated to a product identical with 10-hydroxy-AME in GC-MS/MS analysis and the other one gave rise to 8-hydroxy-AME upon methylation with COMT, indicating which of the two ring A catechols was 10-hydroxy-AOH and which was 8-hydroxy-AOH (Table 1).

From the daughter ion spectrum of the fifth AOH metabolite (Fig. 10), a monohydroxylation product of the methyl

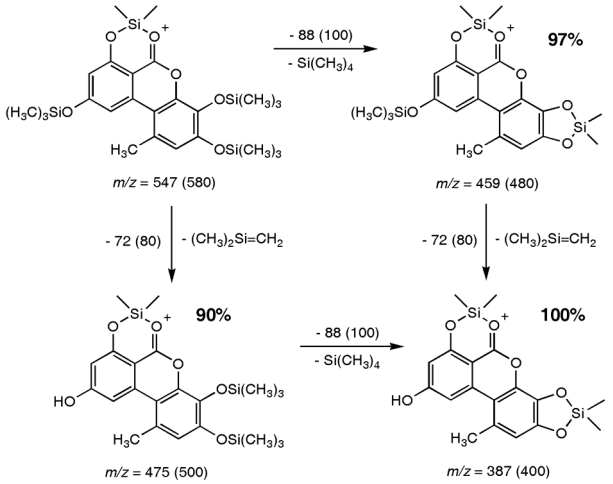

Figure 11. Proposed fragmentation of the $[M-15]^+$ ion (*m/z* 547) of the trimethylsilylated AOH metabolite eventually identified as 4-hydroxy-AOH. Percent values denote relative abundance. Values in parentheses denote *m/z* of the perdeutero-TMS derivative.

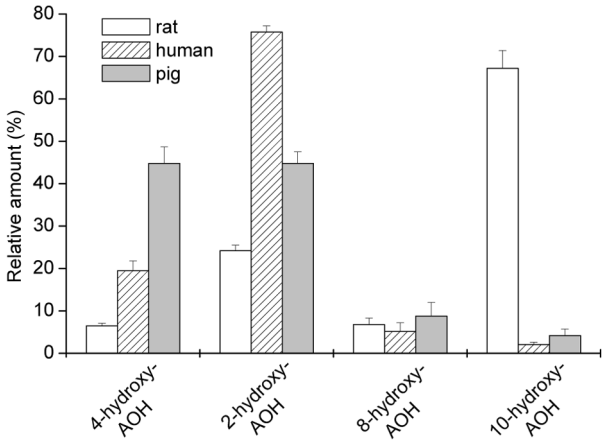

Figure 12. Pattern of oxidative AOH metabolites generated with liver microsomes from rat, human, and pig. The concentration of AOH was 50 μM and did not saturate the hydroxylation reaction. Total formation of hydroxylated metabolites was 228 ± 32.8, 491 ± 26.8, and 128 ± 9.1 pmol/min/nmol cytochrome P450 with microsomes from rat, human, and pig, respectively. Data represent mean ± SD from three independent experiments.

group at C-1 is proposed, which is the only position left for hydroxylation. The ions at *m/z* 457 and 385 can be explained by the elimination of trimethylsilanol (90 amu) from the $[M-15]^+$ ion *m/z* 547, followed by release of $(CH_3)_2Si=CH_2$ (72 amu). If *m/z* 547 loses 72 amu first, the ion at *m/z* 475 is obtained. A second elimination of 72 amu from ion *m/z* 385 explains the ion at *m/z* 313.

Several small peaks eluted after AOH from the HPLC column when the extract of the microsomal incubation of AOH was analyzed (not depicted in Fig. 9). As for AME,

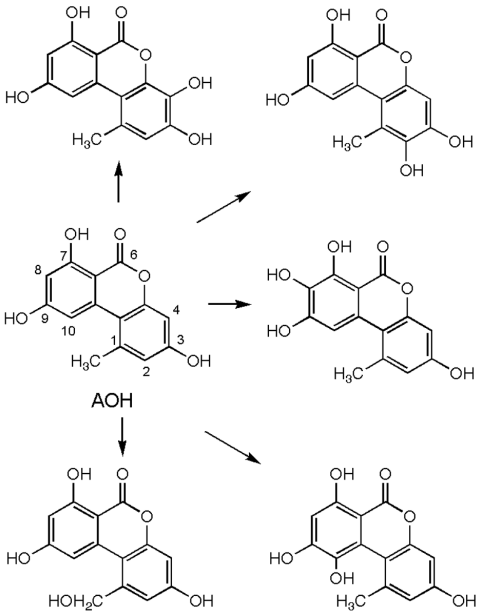

Figure 13. Oxidative metabolism of AOH.

these unpolar products were considered to arise from dimerization of oxidized AOH or metabolites and were not further studied.

When AOH was incubated with human and porcine liver microsomes, the same catechol metabolites were formed as observed with rat liver microsomes although with a different pattern (Fig. 12). In addition, small amounts of the aliphatic hydroxylation product were formed. It is noteworthy that 10-hydroxy-AOH, which is the major metabolite in rat liver microsomes, was only formed in trace amounts in human liver microsomes.

In summary, microsomes from rats, pigs and humans are able to hydroxylate AOH at each conceivable position of the molecule. The four major oxidative metabolites of AOH are catechols (Fig. 13).

4 Discussion

This study has shown that hepatic microsomes from diverse species metabolize AME and AOH preferentially at aromatic positions and, to a minor extent, at the methyl group located at ring C. In addition, AME is demethylated to AOH. The latter reaction is the only pathway in the oxidative metabolism of the *Alternaria* toxins reported in the literature to date [7, 8]. The chemical structures of the novel monohydroxylated metabolites of AME and AOH were mainly elucidated from the daughter ion spectra of the trimethylsilylated derivatives, using both normal and perdeuterated silylating agents. Three types of fragmentation reactions dominated most of the trimethylsilylated metabolites: (i) the formation of a six-membered siloxane ring from the

keto group at C-6 and the trimethylsilyloxyl group at C-7, which is common in compounds with this type of structure, *e. g.*, certain flavones, isoflavones, chalcones, and resorcylic acid lactones [13 – 17], (ii) the formation of a five-membered siloxane ring from two vicinal trimethylsilyloxyl groups, which are common in many catechols [13, 14, 17], (iii) the formation of the same five-membered siloxane ring from a trimethylsiloxyl group and a vicinal methoxyl group, which are frequently encountered in phytochemicals and which also represent the structures of the monoMPs of catechols [14, 17, 18]. Using these typical fragmentations together with information obtained from the products of enzymatic methylation of the microsomal metabolites by COMT, and from comparison with a few authentic reference compounds, chemical structures could be assigned to all the monohydroxylated AME and AOH metabolites. The proposed structures are supported by the chromatographic behavior of the metabolites: in GC, the same sequence was observed for the trimethylsilylated metabolites of AME and AOH, *i. e.*, the 10-hydroxy isomer was eluted first, followed by the 4-hydroxy, 8-hydroxy, and 2-hydroxy isomers (Table 1). In HPLC, the 8-hydroxy isomers preceded the 10-hydroxy isomers and the 4-hydroxy isomers preceded the 2-hydroxy isomers, but the retention times of the ring B and ring A hydroxylation products overlapped in the case of AOH, in contrast to AME (Figs. 2 and 9). The only finding that does not support the assigned structures is the fact that rat liver microsomes prefer C-8 of AME but C-10 of AOH for hydroxylation (Figs. 7 and 12), but this may be a peculiarity of the cytochrome P450 isoforms catalyzing this reaction.

As all the products of aromatic hydroxylation of AME and AOH are either catechols or hydroquinones, which may form reactive semiquinones and quinones or undergo redox cycling, their inactivation by methylation or glucuronidation/sulfation is of considerable toxicological interest. Preliminary experiments in our laboratory have shown that AOH is converted to the MPs of 2- and 4-hydroxy-AOH in precision-cut rat liver slices, which have enzymatic activities for hydroxylation as well as for the methylation of catechols and for glucuronidation/sulfation. These results show that hydroxylation of AOH takes place under *in vivo*-like conditions, *i. e.*, in the presence of competing conjugating pathways. Knowledge of the toxicity and disposition of the oxidative AME and AOH metabolites is mandatory for a better understanding of the health risks posed by these *Alternaria* toxins. For example, mutagenicity has been reported for the parent AME and AOH [3 – 5], and weak estrogenicity has recently been disclosed for AOH [6]. Both properties may be enhanced or attenuated for their metabolites. For studies of their biological activities and further metabolism, the chemical synthesis of the monohydroxylation products of AME and AOH is in progress in one of our laboratories.

This study was supported by the State of Baden-Württemberg (Research Program "Mycotoxins" as part of the State Research Initiative "Food and Health"). We thank Doris Honig for conducting the GC-MS/MS analyses, Timo Gehring and Martina Altemöller for providing alternariol, alternariol methyl ether, as well as graphislactone A and its demethylation products, and Ronald Maul for the LC-MS analyses.

5 References

[1] Scott, P. M., Analysis of agricultural commodities and foods for Alternaria mycotoxins, *J. AOAC Int.* 2001, *84*, 1809 – 1817.

[2] Liu, G. T., Qian, Y. Z., Zhang, P., Dong, Z. M., *et al*., Relationships between Alternaria alternata and oesophageal cancer, *IARC Sci. Publ.* 1991, 258 – 262.

[3] Zhen, Y. Z., Xu, Y. M., Liu, G. T., Miao, J., *et al*., Mutagenicity of Alternaria alternata and Penicillium cyclopium isolated from grains in an area of high incidence of oesophageal cancer – Linxian, China, *IARC Sci. Publ.* 1991, 253 – 257.

[4] Liu, G. T., Qian, Y. Z., Zhang, P., Dong, W. H., *et al*., Etiological role of Alternaria alternata in human esophageal cancer, *Chin. Med. J. (Engl)* 1992, *105*, 394 – 400.

[5] Brugger, E. M., Wagner, J., Schumacher, D. M., Koch, K., *et al*., Mutagenicity of the mycotoxin alternariol in cultured mammalian cells, *Toxicol. Lett.* 2006, *164*, 221 – 230.

[6] Lehmann, L., Wagner, J., Metzler, M., Estrogenic and clastogenic potential of the mycotoxin alternariol in cultured mammalian cells, *Food Chem. Toxicol.* 2006, *44*, 398 – 408.

[7] Pollock, G. A., DiSabatino, C. E., Heimsch, R. C., Coulombe, R. A., The distribution, elimination, and metabolism of 14C-alternariol monomethyl ether, *J. Environ. Sci. Health B* 1982, *17*, 109 – 124.

[8] Olsen, M., Visconti, A., Metabolism of alternariol monomethylether by porcine liver and intestinal mucosa in vitro, *Toxicol. In Vitro* 1987, *2*, 27 – 29.

[9] Koch, K., Podlech, J., Pfeiffer, E., Metzler, M., Total synthesis of alternariol, *J. Org. Chem.* 2005, *70*, 3275 – 3276.

[10] Lake, B. G., Preparation and characterization of microsomal fractions for studies on xenobiotic metabolism, in: Snell, K., Mullach, B. (Eds.), *Biochemical Toxicology: A Practical Approach*, IRL Press, Oxford, UK 1987, pp. 183 – 215.

[11] Bradford, M. M., A rapid and sensitive method for the quantitation of microgram quantities of protein utilizing the principle of protein-dye binding, *Anal. Biochem*. 1976, *72*, 248 – 254.

[12] Omura, T., Sato, R., The carbon monoxide-binding pigment of liver microsomes: I. evidence for its hemoprotein nature, *J. Biol. Chem*. 1964, *239*, 2370 – 2378.

[13] Creaser, C. S., Koupai-Abyazani, M. R., Stephenson, G. R., Mass spectra of trimethylsilyl derivatives of naturally occurring flavonoid aglycones and chalcones, *Org. Mass Spectrom.* 1991, *26*, 157 – 160.

[14] Heinonen, S. M., Hoikkala, A., Wahala, K., Adlercreutz, H., Metabolism of the soy isoflavones daidzein, genistein and glycitein in human subjects. Identification of new metabolites having an intact isoflavonoid skeleton, *J. Steroid Biochem. Mol. Biol*. 2003, *87*, 285 – 299.

[15] Creaser, C. S., Koupai-Abyazani, M. R., Stephenson, G. R., Gas chromatographic-mass spectrometric characterization of flavanones in citrus and grape juices, *Analyst* 1992, *117*, 1105 – 1109.

[16] Kulling, S. E., Honig, D. M., Metzler, M., Oxidative metabolism of the soy isoflavones daidzein and genistein in humans in vitro and in vivo, *J. Agric. Food. Chem.* 2001, *49*, 3024 – 3033.

[17] Pfeiffer, E., Heuschmid, F. F., Kranz, S., Metzler, M., Microsomal hydroxylation and glucuronidation of [6]-gingerol, *J. Agric. Food. Chem.* 2006, *54*, 8769 – 8774.

[18] Harvey, D. J., The mass spectra of the trimethylsilyl derivatives of ginger constituents, *Biomed. Mass Spectrom* 1981, *8*, 546 – 552.

